Z. angew. Math. Phys. 54 (2003) 437–448
0044-2275/03/030437-12
DOI 10.1007/s00033-003-0032-4

Zeitschrift für angewandte Mathematik und Physik ZAMP

Vertical free convective boundary–layer flow in a porous medium using a thermal nonequilibrium model: Elliptical effects

D. A. S. Rees

Abstract. In this paper we study the effect of adopting a two–temperature model of microscopic heat transfer on the classical Cheng & Minkowycz [1] vertical free convection boundary–layer flow in a porous medium. Such a model, which allows the solid and fluid phases not to be in local thermal equilibrium, is found to modify substantially the behaviour of the flow relatively close to the leading edge. A companion paper deals with the (parabolic) boundary–layer theory, but the present work investigates in detail how elliptical effects are manifested. This is undertaken by solving the full equations of motion, rather than the boundary–layer approximation. In general, it is found that at any point in the flow, the temperature of the solid phase is higher than that of the fluid phase, and therefore that the thermal field of the solid phase is of greater extent than that of the fluid phase. The microscopic inter–phase heat transfer is characterised by the coefficient, H, and it is shown that these thermal non–equilibrium effects are strongest when H is small.

Keywords. Boundary layer, porous media, local thermal nonequilibrium, numerical simulation.

Introduction

Free convective boundary–layer flow from a vertical heated surface was considered first by Cheng & Minkowycz [1] who considered various cases where the flow is self–similar. Their analysis, in common with many others which appeared later, assumed that Darcy's law applies, that the Boussinesq approximation is valid, and that the solid and fluid phases comprising the porous medium are in thermal equilibrium locally. In this, and the companion paper, Rees & Pop [2], we investigate the effect of lifting the restriction of local thermal equilibrium between the phases.

Rees & Pop [2] looks at those cases where the boundary–layer approximation is valid, and it is shown there that the boundary–layer splits into two distinct sublayers near the leading edge: a relatively thin sublayer where the fluid temperature adjusts to the ambient temperature, and a relatively thick sublayer where the temperature of the solid phase adjusts to the ambient. The present work extends that boundary–layer analysis by considering flows which are very close to

the leading edge, and this is undertaken by solving the full equations of motion, rather than the boundary–layer approximation to those equations.

Rees & Bassom [3] showed that vertical convection in a semi–infinite medium may be described exactly in terms of the solution of a set of ordinary differential equations if the full equations are written in parabolic coordinates and if local thermal equilibrium is assumed. A later numerical investigation given in Rees [4] into the stability of this flow used the parabolic coordinate system as part of the numerical strategy to simulate unsteady flow. The results of Rees [4], together with those of Lewis, Bassom & Rees [5], indicate very strongly indeed that the vertical free convective flow described in Rees & Bassom [3] is stable. Therefore the present paper is also an extension of Rees [4] into the effects of local thermal nonequilibrium on the stability of the flow, although our main emphasis is on the description of the resulting steady–state flow.

Equations of motion

The equations governing Darcy–Boussinesq convection in a saturated porous medium are usually studied by first invoking the assumption that the solid and fluid phases of the medium are in local thermal equilibrium. In this paper we study one particular case where a two–temperature model of microscopic heat transfer applies. The governing two–dimensional equations are

$$\overline{u}_{\overline{x}} + \overline{v}_{\overline{y}} = 0, \tag{1a}$$

$$\overline{u} = -\frac{K}{\mu}\frac{\partial \overline{p}}{\partial \overline{x}} + \frac{\rho_f g \beta K}{\mu}(T_f - T_\infty), \qquad \overline{v} = -\frac{K}{\mu}\frac{\partial \overline{p}}{\partial \overline{y}}, \tag{1b,c}$$

$$\epsilon(\rho c)_f \frac{\partial T_f}{\partial \overline{t}} + (\rho c)_f \underline{\overline{u}}.\nabla T_f = \epsilon k_f \nabla^2 T_f + h(T_s - T_f), \tag{1d}$$

$$(1-\epsilon)(\rho c)_s \frac{\partial T_s}{\partial \overline{t}} = (1-\epsilon)k_s \nabla^2 T_s - h(T_s - T_f); \tag{1e}$$

see Nield & Bejan [6]. Here, $\overline{u}$ and $\overline{v}$ are the fluid flux velocities in the streamwise (upwards) and cross–stream (horizontal) directions, $\overline{x}$ and $\overline{y}$, respectively, and $\overline{t}$ is the time. The pressure is $\overline{p}$ and the temperature is T, where the f and s subscripts denote the fluid and solid phases, respectively. The following are the other fluid and medium properties: K is the permeability, μ the fluid viscosity, ρ density, c the specific heat, β the coefficient of cubical expansion, ϵ the porosity and k the thermal conductivity. In (1d) and (1e) h is a coefficient which is used to model the microscopic transfer of heat between the fluid and solid phases.

In this paper we shall consider the unsteady two–dimensional flow which is induced by a vertical heated surface held at the constant temperature, T_w, and

embedded in a porous medium with ambient temperature, T_∞, where $T_w > T_\infty$. The pressure may be eliminated by defining a streamfunction, $\overline{\psi}$, according to

$$\overline{u} = \frac{\partial \overline{\psi}}{\partial \overline{y}}, \qquad \overline{v} = -\frac{\partial \overline{\psi}}{\partial \overline{x}}, \tag{2}$$

and equations (1) reduce to the following

$$\frac{\partial^2 \overline{\psi}}{\partial \overline{x}^2} + \frac{\partial^2 \overline{\psi}}{\partial \overline{y}^2} = \frac{\rho_f g \beta K}{\mu} \frac{\partial T_f}{\partial \overline{y}} \tag{3a}$$

$$\epsilon(\rho c)_f \frac{\partial T_f}{\partial \overline{t}} + (\rho c)_f \Big(\frac{\partial \overline{\psi}}{\partial \overline{y}} \frac{\partial T_f}{\partial \overline{x}} - \frac{\partial \overline{\psi}}{\partial \overline{x}} \frac{\partial T_f}{\partial \overline{y}} \Big) = \epsilon k_f \Big(\frac{\partial^2 T_f}{\partial \overline{x}^2} + \frac{\partial^2 T_f}{\partial \overline{y}^2} \Big) + h(T_s - T_f), \tag{3b}$$

$$(1-\epsilon)(\rho c)_s \frac{\partial T_s}{\partial \overline{t}} = (1-\epsilon) k_s \Big(\frac{\partial^2 T_s}{\partial \overline{x}^2} + \frac{\partial^2 T_s}{\partial \overline{y}^2} \Big) - h(T_s - T_f). \tag{3c}$$

These equations need to be nondimensionalised in a different way from that of Rees & Pop [2] as we do not invoke the boundary–layer approximation. If we define R to be

$$R = \frac{(\rho c)_f \rho_f g \beta K (T_w - T_\infty)}{[(1-\epsilon)k_s + \epsilon k_f]\mu}, \tag{4}$$

where we note that the term in square brackets in the denominator is the equivalent conductivity of the saturated medium, then R multiplied by a lengthscale is a porous medium Rayleigh number. In (4) T_w is the uniform wall temperature and T_∞ is the ambient fluid temperature where $T_w > T_\infty$. Now we introduce the scalings,

$$\overline{x} = x/R, \qquad \overline{y} = y/R, \qquad \overline{t} = \frac{(\rho c)_f}{R^2 k_f} t, \tag{5a,b,c}$$

$$\overline{\psi} = \frac{\epsilon k_f}{(\rho c)_f} \psi, \qquad T_f = (T_w - T_\infty)\theta + T_\infty, \qquad T_s = (T_w - T_\infty)\phi + T_\infty, \tag{5d,e,f}$$

into equations (3) to yield,

$$\frac{\partial^2 \psi}{\partial x^2} + \frac{\partial^2 \psi}{\partial y^2} = \Big(1 + \frac{1}{\gamma}\Big) \frac{\partial \theta}{\partial y}, \tag{6a}$$

$$\frac{\partial \theta}{\partial t} = \frac{\partial^2 \theta}{\partial x^2} + \frac{\partial^2 \theta}{\partial y^2} + \frac{\partial \psi}{\partial x}\frac{\partial \theta}{\partial y} - \frac{\partial \psi}{\partial y}\frac{\partial \theta}{\partial x} + H(\phi - \theta), \tag{6b}$$

$$\alpha \frac{\partial \phi}{\partial t} = \frac{\partial^2 \phi}{\partial x^2} + \frac{\partial^2 \phi}{\partial y^2} - \gamma H(\phi - \theta). \tag{6c}$$

In equations (6) the three parameters, H, γ and α, are given by

$$H = \frac{h}{\epsilon k_f R^2}, \qquad \gamma = \frac{\epsilon}{1-\epsilon}\frac{k_f}{k_s}, \qquad \alpha = \frac{k_f}{k_s}\frac{(\rho c)_s}{(\rho c)_f}. \tag{7}$$

H is a scaled microscopic inter–phase rate of heat transfer which was assumed in Rees & Pop [2] to be asymptotically small, γ is a porosity–scaled conductivity ratio, and α is a diffusivity ratio.

Following Rees [4] we transform equations (6) into parabolic coordinates using

$$x = (\xi^2 - \eta^2)/4, \qquad y = \xi\eta/2, \tag{8}$$

to obtain

$$\frac{\partial^2\psi}{\partial\xi^2} + \frac{\partial^2\psi}{\partial\eta^2} = \Big(1 + \frac{1}{\gamma}\Big)\Big[\frac{\xi}{2}\frac{\partial\theta}{\partial\eta} + \frac{\eta}{2}\frac{\partial\theta}{\partial\xi}\Big], \tag{9a}$$

$$\frac{(\xi^2+\eta^2)}{4}\Big[\frac{\partial\theta}{\partial t} + H(\theta-\phi)\Big] = \frac{\partial^2\theta}{\partial\xi^2} + \frac{\partial^2\theta}{\partial\eta^2} + \frac{\partial\psi}{\partial\xi}\frac{\partial\theta}{\partial\eta} - \frac{\partial\psi}{\partial\eta}\frac{\partial\theta}{\partial\xi}, \tag{9b}$$

$$\frac{(\xi^2+\eta^2)}{4}\Big[\alpha\frac{\partial\phi}{\partial t} + \gamma H(\phi-\theta)\Big] = \frac{\partial^2\phi}{\partial\xi^2} + \frac{\partial^2\phi}{\partial\eta^2}. \tag{9c}$$

One of the chief results of [2] is that all boundary layer flows approach a self–similar form at very large distances from the leading edge, and that they all have identical thickness. The present nondimensionalisation is such that the large–ξ steady solutions of equations (9) are likewise of equal thickness, and this allows different cases to be compared easily.

The boundary conditions required to complete the specification of the problem are that $\psi = 0$, $\theta = \phi = 1$ on $\eta = 0$; $\psi = \theta_\xi = \phi_\xi = 0$ on $\xi = 0$; $\psi_\eta = \theta = \phi = 0$ on $\eta = \eta_{\max}$; and $\psi_\xi = \theta_\xi = \phi_\xi = 0$ on $\xi = \xi_{\max}$.

Numerical methodology

The solution of equations (9) was undertaken using a suitably modified version of the method described in [3]. The equations were discretised in both the ξ and η directions using second–order accurate central differences and the nonlinear terms in (9b) were approximated using Arakawa's formulation, see [7], one which is ideally suited to long–term evolution studies. However, a first-order accurate backward difference in time was used to obtain an fully implicit scheme. This scheme is unconditionally stable, subject to being able to compute the solutions at each timestep, and has much better stability properties than a more conventional second–order accurate scheme based on the Crank–Nicolson method. For when the timestep is relatively large, backward–difference solutions of, say, the two–dimensional Fourier equation,

$$\frac{\partial\chi}{\partial t} = \frac{\partial^2\chi}{\partial x^2} + \frac{\partial^2\chi}{\partial y^2}, \tag{10}$$

exhibit monotonic decay to the ultimate steady state, whereas the corresponding solution using Crank–Nicolson exhibits pointwise oscillations which decay only very slowly.

In the present problem, the coefficient of the Laplacian terms in equations (9b) and (9c) varies with ξ and η, and may be thought of as a spatially–varying thermal diffusivity. From a numerical point of view this means that the flow adjusts very quickly near the leading edge, and very slowly far downstream. Again, the presence of such coefficients rules out any possibility of using an explicit scheme for solving (9). Without these coefficients the maximum useable timestep is proportional to the square of the spatial step, but with them the timestep is proportional to the fourth power. Likewise, locations very near the leading edge in (9) are equivalent to having very large timesteps in the solution to equation (10), and therefore pointwise oscillations in the evolving solution are expected near the leading edge when solving (9) using a method based on the Crank–Nicolson scheme. Therefore we adopted the backward–difference discretisation. Indeed, given that the final state of all cases considered is that steady flow prevails, the freedom to modify the timestep to make efficient use of the CPU time available was also an important consideration.

If we define t_n to be the n^{th} timestep, ξ_i, the i^{th} grid point in the ξ–direction, η_j, the j^{th} gridpoint in the η–direction, and $\chi^n_{i,j}$ to be the value of the typical variable, χ at these points, then the full difference equations corresponding to equations (9) are

$$\frac{\psi^{n+1}_{i+1,j} - 2\psi^{n+1}_{i,j} + \psi^{n+1}_{i-1,j}}{\delta\xi^2} + \frac{\psi^{n+1}_{i,j+1} - 2\psi^{n+1}_{i,j} + \psi^{n+1}_{i,j-1}}{\delta\eta^2} = \left(1 + \frac{1}{\gamma}\right)\left[\frac{\xi_i}{2}\frac{\theta^{n+1}_{i,j+1} - \theta^{n+1}_{i,j-1}}{2\delta\eta} + \frac{\eta_j}{2}\frac{\theta^{n+1}_{i+1,j} - \theta^{n+1}_{i-1,j}}{2\delta\xi}\right], \quad (11a)$$

$$\frac{(\xi_i^2 + \eta_j^2)}{4}\left[\frac{\theta^{n+1}_{i,j} - \theta^{n}_{i,j}}{\delta t} + H(\theta^{n+1}_{i,j} - \phi^{n+1}_{i,j})\right] = \frac{\theta^{n+1}_{i+1,j} - 2\theta^{n+1}_{i,j} + \theta^{n+1}_{i-1,j}}{\delta\xi^2} + \frac{\theta^{n+1}_{i,j+1} - 2\theta^{n+1}_{i,j} + \theta^{n+1}_{i,j-1}}{\delta\eta^2} + \mathcal{L}(\psi^{n+1}_{i,j}, \theta^{n+1}_{i,j}), \quad (11b)$$

$$\frac{(\xi_i^2 + \eta_j^2)}{4}\left[\alpha\frac{\phi^{n+1}_{i,j} - \phi^{n}_{i,j}}{\delta t} - \gamma H(\theta^{n+1}_{i,j} - \phi^{n+1}_{i,j})\right] = \frac{\phi^{n+1}_{i+1,j} - 2\phi^{n+1}_{i,j} + \phi^{n+1}_{i-1,j}}{\delta\xi^2} + \frac{\phi^{n+1}_{i,j+1} - 2\phi^{n+1}_{i,j} + \phi^{n+1}_{i,j-1}}{\delta\eta^2}, \quad (11c)$$

where $\mathcal{L}(\psi^{n+1}_{i,j}, \theta^{n+1}_{i,j})$ is the Arakawa [7] formulation of the discretised Jacobian:

$$\mathcal{L}(\psi_{i,j}^{n+1},\theta_{i,j}^{n+1}) = \Big[\big(\psi_{i+1,j}^{n+1}-\psi_{i-1,j}^{n+1}\big)\big(\theta_{i,j+1}^{n+1}-\theta_{i,j-1}^{n+1}\big)- \big(\psi_{i,j+1}^{n+1}-\psi_{i,j-1}^{n+1}\big)\big(\theta_{i+1,j}^{n+1}-\theta_{i-1,j}^{n+1}\big) + \psi_{i+1,j}^{n+1}\big(\theta_{i+1,j+1}^{n+1}-\theta_{i+1,j-1}^{n+1}\big)-\psi_{i-1,j}^{n+1}\big(\theta_{i-1,j+1}^{n+1}-\theta_{i-1,j-1}^{n+1}\big) - \psi_{i,j+1}^{n+1}\big(\theta_{i+1,j+1}^{n+1}-\theta_{i-1,j+1}^{n+1}\big)+\psi_{i,j-1}^{n+1}\big(\theta_{i+1,j-1}^{n+1}-\theta_{i-1,j-1}^{n+1}\big) + \theta_{i,j+1}^{n+1}\big(\psi_{i+1,j+1}^{n+1}-\psi_{i-1,j+1}^{n+1}\big)-\theta_{i,j-1}^{n+1}\big(\psi_{i+1,j-1}^{n+1}-\psi_{i-1,j-1}^{n+1}\big) - \theta_{i+1,j}^{n+1}\big(\psi_{i+1,j+1}^{n+1}-\psi_{i+1,j-1}^{n+1}\big) + \theta_{i-1,j}^{n+1}\big(\psi_{i-1,j+1}^{n+1}-\psi_{i-1,j-1}^{n+1}\big)\Big]/12\delta\xi\,\delta\eta. \tag{12}$$

Here the timestep, and steplengths in the ξ and η directions are given by δt, $\delta\xi$ and $\delta\eta$, repsectively.

At each timestep the resulting finite difference equations were solved using the line–relaxation Gauss–Seidel method coupled with the Full Approximation Scheme multigrid method with V–cycling; see Brandt [8]. Typically each computation was initiated using the steady θ solution corresonding to the local thermal equilibrium solution presented by Rees & Bassom [3], with ϕ being set equal to θ, and ψ set to zero. The use of a backward–difference method means that ψ does not have to be prescribed at the outset. The appropriate initial θ–profile was computed using the same code, but a decaying profile was used as its initial condition. Indeed, the present code may be used for this purpose by setting $H = 0$, thereby decoupling the θ and ϕ equations, and setting the coefficient of the right–hand–side of (9a) to be unity. The solutions obtained for ψ and ϕ are irrelevant, and are discarded. A crude form of timestep control allowed the timestep to increase as the computation approaches the steady–state; we used the same methodology as Rees & Bassom [9] but typically used a maximum timestep of 10 to ensure that the Gauss–Seidel/multigrid iteration scheme converges.

In the computation we used 128 intervals in the ξ–direction and 32 in the η–direction. Further efficiency can be gained by using a nonuniform grid, or equivalently, a coordinate–stretching transformation. The latter will, of course, modify equations (9), but this is a straightforward change, and its details are omitted here. In the ξ–direction we use the same transformation as in [4], whereas η is modified by using $\eta = e^{\eta^*}$ where η^* is the new variable. In our computations we took $0 \le \xi \le 55$ (equivalent to $0 \le x \le 756.25$ on the heated surface), and $0 \le \eta^* \le 4$ (equivalent to $0 \le \eta \le e^4 \simeq 55.6$). In the η–direction grid points are concentrated mainly towards $\eta = 0$, the gridpoint nearest to the heated surface being located at $\eta = 0.133$.

In each case the code was run until the maximum pointwise change in θ between the timesteps was less than 10^{-6}. This criterion was always satisfied after the timestep had achieved its maximum value.

Numerical Results

There are two main parameters to vary, H and γ. Although a third parameter, α, appears in the governing equations, it multiplies a time–derivative, and therefore it affects only the evolution to the steady-state flow and not the steady–state flow itself. In all the computations presented here we set $\alpha = 1$, although other choices of α yield identical steady–state results. The results of our computations are displayed in the form of isotherm plots in Figures 1 and 2, and in the form of surface rates of heat transfer in Figures 3 and 4.

Figure 1 displays how the thermal field of both the solid and fluid phases changes as H is reduced when $\gamma = 1$. When $H = 1$ there is little difference between the θ and ϕ solutions and we can say in this case that the flow is essentially in local thermal equilibrium except, perhaps, at locations very close indeed to the leading edge (see also the $H = 1$ curves in Figure 3). As H decreases towards zero, nonequilibrium effects become stronger, especially near the leading edge, and these effects become increasingly noticeable further downstream of the leading edge. When H is as small as 0.001, the thermal field of the solid phase has acquired a distinctive shape relatively close to the leading edge. Firstly, at locations below the leading edge, the solid–phase isotherms are nearly horizontal for a substantial distance before turning upwards. Secondly, these isotherms are nearly vertical at and just above $x = 0$ and lie well outside the temperature field of the fluid phase; both these phenomena are entirely consistent with the boundary–layer theory presented in [2] — see Figure 2 of that paper. The main conclusion to be drawn is that, when H is small, temperature differences between the phases are to be expected because of the relatively weak transfer of heat between the phases. Thus heat conduction appears to be relatively strong in the solid phase and is not affected greatly by the advection of heat in the fluid phase. Conversely, when H is large, temperature differences between the phases cannot be sustained in the steady state.

In Figure 2 we show how variations in γ change the temperature field when $H = 0.01$. As γ increases from 1.0 the temperature difference between the phases becomes smaller — this may be explained by appealing to the fact that γ multiplies the temperature–difference term in equation (9c), and therefore the solid phase tries to minimise the temperature difference between the phases when γ is large. Thus variations in γ seem to have the same qualitative effect on the flow as do variations in H. However, when γ is very small, we can see that there is an accompanying change in the thickness of the fluid temperature field near $x = 0$, which is also decreasing as γ decreases. The isotherms themselves also have a marked change in their general appearance near the leading–edge. In Rees & Pop [2] we showed, using asymptotic theory, that the fluid boundary–layer thickness near the leading edge is independent of γ and that it eventually thickens to a γ–dependent value at large distances. But in that paper the fluid conductivity was used in the nondimensionalisation process, whereas here we use the effective

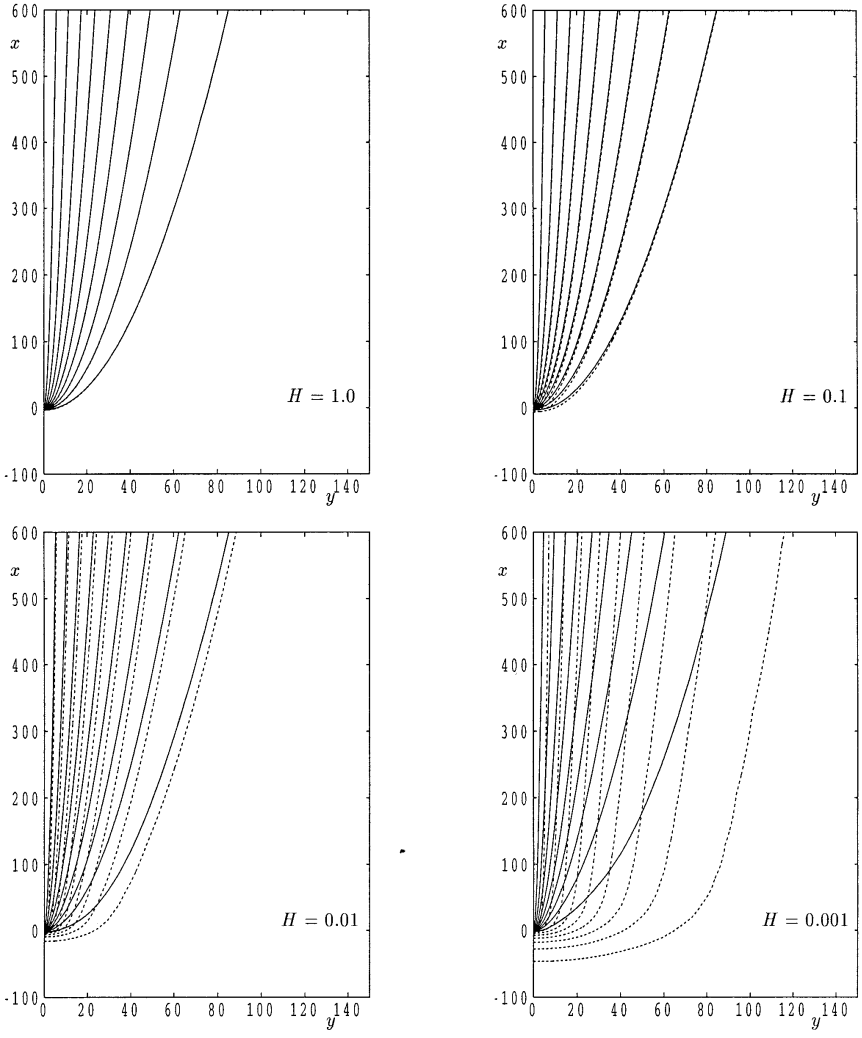

Figure 1. Isotherms for both the fluid phase (solid lines) and solid phase (dashed lines) for $\gamma = 1.0$ for various values of H.

conductivity of the medium, where the ratio between these conductivities is $1+\gamma^{-1}$. Thus all flows here attain the same thickness in terms of η at large distances from the leading edge, but when γ becomes small the near–leading edge thickness decreases.

Figures 3 and 4 depict the numerical values of $Q_f = -\partial\theta/\partial\eta$ and $Q_s = -\partial\phi/\partial\eta$

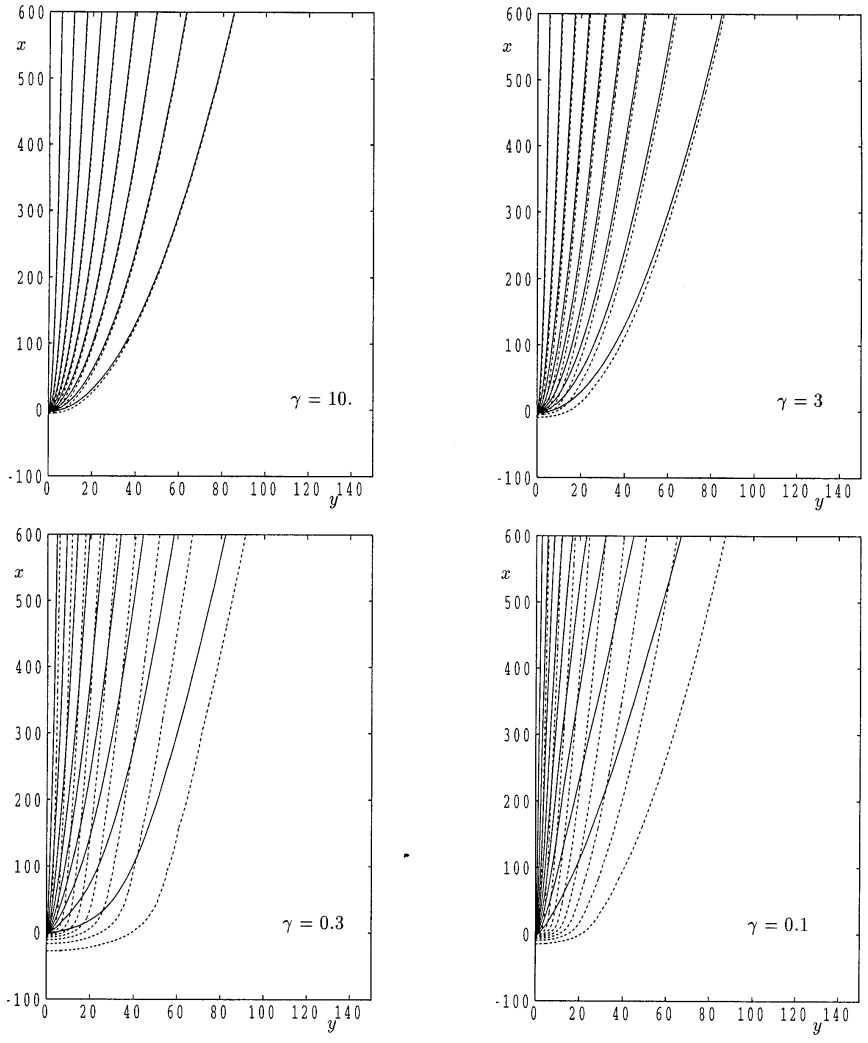

Figure 2. Isotherms for both the fluid phase (solid lines) and solid phase (dashed lines) for $H = 0.01$ for various values of γ. The isotherm plot for $\gamma = 1$ is presented in Figure 1.

at $\eta = 0$ for $\xi \geq 0$, although these values are plotted against the physical variable x. Figure 3 corresponds to the isotherm plots shown in Figure 1, and Figure 4 to those shown in Figure 2. Also shown in Figure 1 is the rate of heat transfer for the datum case of Rees [4] where the rate of heat transfer is independent of x; this corresponds to $H \to \infty$.

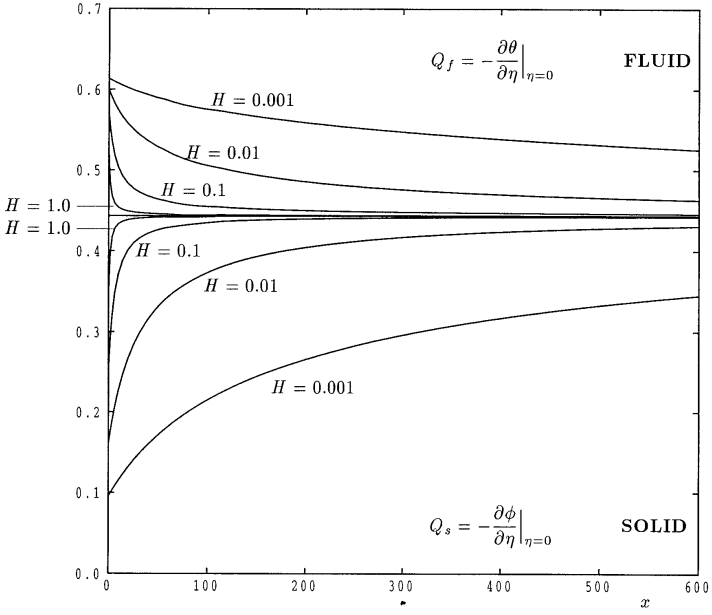

Figure 3. Variation with x of Q_f and Q_s, the surface rates of heat transfer for the fluid and solid phases, respectively, for $\gamma = 1.0$, and for $H = 1.0$, $H = 0.1$, $H = 0.01$ and $H = 0.001$. The horizontal line corresponds to the datum case where the medium is in local thermal equilibrium.

It is clear from Figure 3 that the fluid rate of heat transfer, Q_f, is always greater than Q_s, the solid rate of heat transfer. Again this qualitative detail is in accord with the conclusions of Rees & Pop [2]. In fact Q_f is always greater than that corresponding to the datum case, and Q_s is less. The degree of departure from the datum case can be regarded as a measure of the degree to which nonequilibrium effects are important. Therefore we can see clearly that the influence of nonequilibrium effects spreads rather quickly downstream as H decreases from 1, and the maximum extent of departure from equilibrium also increases. When $H < 0.01$ thermal nonequilibrium exists quite strongly throughout the whole computational domain, and therefore it may be possible that the use of a larger computational domain will change the $H = 0.001$ solution presented here. However, we do not think that such changes will be particularly large, for the flow is essentially parabolic near the outflow boundary, and therefore much more dependent on upstream conditions than those prevailing downstream.

Figure 4 shows that Q_f and Q_s are both very sensitively dependent on the value of γ, with the value of Q_f being more sensitive.

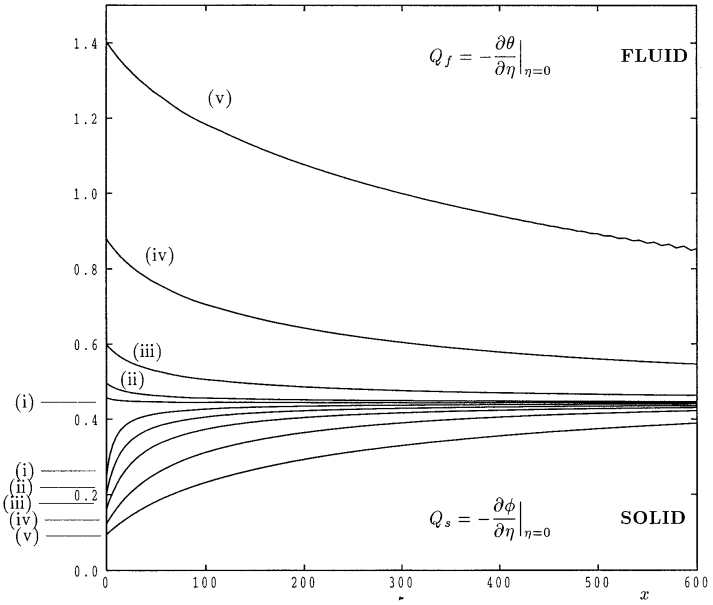

Figure 4. Variation with x of Q_f and Q_s, the surface rates of heat transfer for the fluid and solid phases, respectively, for $H = 0.01$, and for (i) $\gamma = 10$, (ii) $\gamma = 3$, (iii) $\gamma = 1$, (iv) $\gamma = 0.3$ and (v) $\gamma = 0.1$.

Conclusions

In this paper we have sought to identify how thermal nonequilibrium effects serve to modify the flow induced by a constant temperature vertical surface embedded in a porous medium. The companion paper, Rees & Pop [2], presents a formal boundary–layer theory which indicates, among other things, that nonequilibrium effects are most pronounced near the leading edge. The present paper extends that work by reinstating elliptic effects. Thus the full equations of motion are solved numerically and a detailed study of the flow near the leading edge obtained. While a comprehensive quantitative comparison between the two works has not been undertaken, due to the necessity of taking very small values of H, and of having a correspondingly large computational domain, an excellent qualitative agreement has been found when H is sufficiently small. In particular, the boundary–layer theoretical solution given in Figure 2 of [2] yields a solid–phase set of isotherms which appear to terminate at non–zero values of y at $x = 0$, unlike those of the fluid phase. The present numerical investigation shows that this rather unusual behaviour for a boundary–layer is consistent with the solution of the fully ellip-

tic equations shown in the present Figure 2. This agreement also lends further credence to the validity of the analysis presented in [2].

A very important conclusion from the present numerical work is that these flows are likely to be stable since the steady flows presented have been obtained using unsteady simulations. The stability of the case where local thermal equilibrium applies was demonstrated by the combined numerical study of Rees [4] and asymptotic study of Lewis et al. [5]. A definitive statement about the stability of the present flows will require a similar asymptotic analysis to be undertaken.

References

[1] Cheng, P., Minkowycz, W.J., Free convection about a vertical flat plate embedded in a porous medium with application to heat transfer from a dike, *J. Geophys. Res.* **82** (1977), 2040-2044.
[2] Rees, D.A.S., Pop, I., Vertical free convective boundary–layer flow in a porous medium using a thermal nonequilibrium model, *Journal of Porous Media* **3** (2000), 31-44.
[3] Rees, D.A.S., Bassom, A.P., Some exact solutions for free convective flows over heated semi-infinite surfaces in porous media, *Int. J. Heat Mass Transfer* **34** (1991), 1564-1567.
[4] Rees, D.A.S., Nonlinear wave stability of vertical thermal boundary layer flow in a porous medium, *J. Appl. Math. Phys.* **44** (1993), 306-313.
[5] Lewis, S., Bassom, A.P., Rees, D.A.S., The stability of vertical thermal boundary layer flow in a porous medium, *Eur. J. Mech. B: Fluids* **14** (1995), 395–408.
[6] Nield, D.A., Bejan, A., *Convection in Porous Media* (2nd ed.). Springer, New York, 1998.
[7] Arakawa, A., Computational design of long–term numerical integration of the equations of fluid motion: I. Two–dimensional incompressible flow, *J. Comp. Phys.* **1** (1966), 119–143.
[8] Brandt, A., Multigrid techniques: 1984 guide with applications to fluid dynamics. *Lecture notes in C.F.D.* at the Von Karman Institute for Fluid Dynamics.. Published by G.M.D. mbH, Bonn as *GMD–Studien* **85**, 1984.
[9] Rees, D.A.S., Bassom, A.P., The nonlinear nonparallel wave instability of free convection induced by a horizontal heated surface in fluid-saturated porous media, *Journal of Fluid Mechanics* **253** (1993), 267–296.

D. A. S. Rees
Department of Mechanical Engineering
University of Bath
Bath BA2 7AY
U.K.

(Received: April 10, 2000)